RSC Advances

PAPER

View Article Online
View Journal | View Issue

Cite this: *RSC Adv.*, 2022, **12**, 33653

Titanium dioxide incorporated in cellulose nanofibers with enhanced UV blocking performance by eliminating ROS generation†

Iqra Rabani,[a] Ha-Na Jang,[a] Ye-Jee Park,[a] Muhammad Shoaib Tahir,[a] Yun-Bi Lee,[a] Eun-Yi Moon,[b] Jin Won Song[c] and Young-Soo Seo *[a]

The preparation of sunblocks with dispersion stability, ultraviolet blocking, and photocompatibility remains a considerable challenge. Plant-derived natural polymers, such as cellulose nanofibers (CNF), show versatile traits, including long aspect ratio, hydrophilic nature, resource abundance, and low material cost. In the present study, a facile and cost-effective strategy is reported for the fabrication of nanostructured inorganic materials by incorporating natural polymers as interspersed, systematically nanosized titanium dioxide (TiO_2) particles onto CNF. Among all experiments, the optimized TiO_2@CNF3 showed higher ultraviolet blocking performance and less whitening effect. The outstanding performance is attributed to the engineering of equally dispersed nano-sized TiO_2 particles on the CNF surface and stable dispersion. Significantly, TiO_2@CNF3 exhibited excellent compatibility with avobenzone (80%), an oil-soluble ingredient used in sunblock products, illustrating the photoprotection enhancement under ultraviolet A (UVA) and ultraviolet B (UVB). Moreover, only 14.8% rhodamine B (Rho-B) dye degraded through photocatalytic oxidation process with the TiO_2@CNF3, which is negligible photocatalytic activity compared to that of TiO_2 (95% dye degraded). Furthermore, commercial inorganic and organic sunblock products with SPF lifetimes of 35^+ and 50^+ were modified using CNF, significantly enhancing the transmittance performance compared to that of the pure sunblock. However, it was also observed that hydrophilic CNF tended to demulsify the creams due to electrostatic disequilibrium. This CNF-based modified TiO_2 system is a new window to replace effective sunblock products in high-value-added applications, such as cosmetics.

Received 12th October 2022
Accepted 14th November 2022

DOI: 10.1039/d2ra06444h

rsc.li/rsc-advances

1. Introduction

Long-term exposure to ultraviolet (UV) radiation causes severe damage to humans, such as skin burns and cancer.[1] In this regard, antioxidants can be considered promising candidates for enhancing the endogenous capacity of the skin by neutralizing reactive oxygen species (ROS) induced by external factors, such as UV radiation. Therefore, antioxidants, along with UV-blocking agents, are vital ingredients in many skin care products. To effectively block UV radiation, both inorganic and organic materials have been developed based on the UV-blocking mechanism. During the last few decades, considerable attention has been given to the development of UV photoprotective materials, especially inorganic UV blockers that is, zinc oxide (ZnO), silicon dioxide (SiO_2), aluminum oxide (Al_2O_3), and titanium dioxide (TiO_2) embedded in a polymer matrix[2–4] that can absorb UV radiation and exhibit good stability. Nano-sized TiO_2-based photoprotectors are extensively employed in sunblock products as inorganic UV blockers because they can scatter and reflect ultraviolet A (UVA) (320–400 nm) and ultraviolet B (UVB) (280–320 nm) in sunlight. Moreover, they are cost-effective, environmentally friendly, durable, and chemically and thermally stable, with low toxicity and a wider shielding range.[5,6]

Under sunlight, the use of TiO_2 nanoparticles has been limited in cosmetics because of their notable photocatalytic activity, which can damage cellular components, such as lipids, proteins, and DNA.[7–11] To eliminate the photocatalytic activity of TiO_2 nanoparticles, many studies have focused on fabricating hybrids such as illite/TiO_2,[12] TiO_2@fabric,[13] and lignin/TiO_2 [14] and TiO_2 coated with silica shells.[15,16] However, excessive inorganic coating leads to poor light absorption and transmittance in UV blockers, eventually hindering their application in skin care products. Instead, various di- and triblock copolymers, such as poly(methyl methacrylate-*b*-acrylic acid) and poly(-ethylene oxide)-*b*-poly(2-(dimethylamine)ethyl methacrylate)-*b*-poly(styrene), have been used to reduce the photocatalytic

[a]*Interface Lab, Department of Nanotechnology and Advanced Materials Engineering, Sejong University, Seoul 05006, Korea. E-mail: ysseo@sejong.ac.kr*
[b]*Department of Bioscience and Biotechnology, Sejong University, Seoul 05006, Korea*
[c]*Fine Lab Co., Ltd., 97 Sinilseo-ro 126 beon-gil, Daedeok-gu, Daejeon, Korea*

† Electronic supplementary information (ESI) available. See DOI: https://doi.org/10.1039/d2ra06444h

activity without sacrificing the UV-blocking performance.[17,18] The drawbacks of these block copolymers are that the synthesis process is complex and expensive, and the rising demand for biodegradability and biocompatibility has led to the consideration of using natural materials as substitutes for synthetic materials.

In recent years, natural sunblock products have gained considerable attention. Natural products such as *Rosa kordesi*, extract of *Carica papaya*, green coffee oil, and *Helichrysum arenarium* are proven to have a reasonable UV radiation protection function.[19–22] In-demand natural sunblock is prepared using natural ingredients that are often expensive and commercially limited on a global scale. Cellulose nanofiber (CNF) (a few microns long and ~10 nm wide) fabricated from cellulose, which is the most abundant natural polymer, is a renewable "green" material that is easily dispersed in water due to its hydrophilic nature.[23] It can be used as a moisturizer and dispersive agent for nanoparticles.[24] CNF have never been used as sunblock in cosmetics. The high-end large-scale application of industrial CNF is still under exploration. Therefore, CNF with TiO_2 as a photoprotective material may be a viable option in the cosmetics field.

The objective of this work was to prepare uniformly dispersed nanosized TiO_2 nanoparticles (NPs) on the surface of CNF by employing a simple and facile sol–gel reaction and to investigate the properties of the sunblock. The introduction of TiO_2 NPs onto the CNF surface resulted in a higher UV shielding performance, even at low quantities of TiO_2 due to good dispersion. The photocatalytic activity of the TiO_2@CNF composite and pristine TiO_2 was examined using rhodamine B (Rho-B) as a model contaminant under UVA and UVB illumination, confirming that the composite exhibits a significantly lower photocatalytic effect than that of pristine TiO_2. In addition, its photostability was studied by blending with avobenzone (Avb), which is a representative organic UV blocker. More than 80% photoprotection was observed for the composite, whereas 60% was observed for pristine TiO_2 particles after UVA and UVB illumination, indicating remarkable photoprotection. This new hybrid is a promising option for improving sunblock performance in cosmetics. Additionally, the transmittance performance of four commercial sunblock products with SPF lifetimes of 50^+ and 35^+ were tested by blending with CNF. As expected, CNF enhanced the transmittance performance of the local sunblock products because of its good dispersion. Although the underlying mechanism remains to be elucidated, it was attributed to the synergistic effect between the CNF and TiO_2 particles in the lotions, as well as the hydrophilic property of CNF.

2. Experimental detail

2.1 Materials

Absolute ethanol (CH_3CH_2OH, 98.0%, $M_W = 46.07$) and diethanolamine ($HN(CH_2CH_2OH)_2$, 98.0%, $M_W = 105.14$) were obtained from Sigma Aldrich. Titanium tetra-*n*-butoxide ($((CH_3CH_2CH_2CH_2O)_4Ti$, 97.0%, $M_W = 340.32$ g mol^{-1}) was purchased from the Chuo-ku (Tokyo, Japan). CNF was directly purchased by Moorim P&P (Ulsan, Korea). They have produced the CNF through re-fined method, which is white odorless gel with 2.2 wt% solid content. In addition, the full length and width of the fiber was approximately 100 μm and 50 nm, respectively.

2.2 Synthesis method of the TiO_2@CNFx nanocomposite

TiO_2 NPs were synthesized on the CNF surface using a facile and cost-effective sol–gel process. The sol–gel synthesis layout is presented in the ESI.† Titanium tetra-*n*-butoxide (TBT) and diethanolamine (DEA) were added dropwise into the CNF ethanol solution at a concentration of 5 mg mL^{-1} at 60 °C under continuous stirring for two hours (h). The white precipitate was separated by centrifugation and washed three times with ethanol and deionized (DI) water to ensure the removal of undissolved impurities. The sample was dried in a convection oven at 100 °C overnight and named the TiO_2@CNF hybrid. The prepared samples were stored in a desiccator for further analysis.

In addition, pristine TiO_2 NPs were synthesized using the conventional sol–gel process, as described earlier.[25] Briefly, stoichiometric amounts of the starting materials, that is, TBT (5 mL) and DEA (1.5 mL), were dissolved in 50 mL of ethanol with continuous stirring for 2 h at 60 °C. White precipitates were obtained using vacuum filtration. The samples were washed three times with a water and ethanol mixture (1 : 2 by volume) to remove undesired impurities. The resulting samples were stored in a desiccator.

2.3 Dispersion stability test

DI water was added to approximately 0.1 and 0.5 wt% quantities of pristine TiO_2 and TiO_2@CNF hybrid, respectively. The suspension was then homogenized using an ultrasound for 5 min. Finally, all the samples were maintained for approximately 24 h.

2.4 Preparation of CNF based sunblock

Four inorganic and organic sunblock products with SPF lifetimes of 35^+ and 50^+ were purchased from manifold companies as follows: "HERA Sun Mate daily" (35^+, inorganic sunblock 1, ioSB1), "The Face shop" (50^+, inorganic sunblock 2, ioSB2), "MediFlower" (50^+, organic sunblock 1, oSB1), and "V10 UV shield" (50^+, organic sunblock 2, oSB2). Then, each sunblock was blended with CNF as follows: 1.90 g of sunblock was mixed with 3 or 5 g of CNF (2 wt%) hydrogel and the concentration of the sunblock was adjusted to 0.1 and 0.2 mg mL^{-1} by adding DI water with magnetic stirring overnight. The transmittance was then measured using a UV-visible (vis) spectrometer. Detailed information regarding the active and inactive ingredients of the inorganic and organic sunblock is provided in the ESI, S2–S5.†

2.5 Photocatalytic test

The photocatalytic and photolysis activities were validated using a photoreactor consisting of a combination of 12 UVA and UVB lamps with 48 W power. Approximately 2 mL of an aqueous

suspension of rhodamine-B (Rho-B) with an initial concentration of 0.026 wt% and a specific quantity of as-prepared catalyst (5 mg) were mixed in a 40 mL quartz beaker and stored for 3600 s under UVA and UVB light, respectively. After that, 3 mL of the aqueous suspension was withdrawn every 1 h, and then the samples were immediately centrifuged at 7000 rpm for 10 min at 20 °C. The supernatants were trickled through a pre-cleaned 0.2 μm membrane filter (cellulose acetate; Advantech, Japan). The maximum absorbance of Rho-B was measured at a wavelength of 555 nm using a UV-vis-NIR spectrophotometer (Cary 5000). The degradation efficiency (%) of Rho-B was evaluated using the following equation: % degradation $= 100 \times \frac{C_o - C_t}{C_o}$, where C_o is the concentration at time $t = 0$ and C_t is the concentration after the treatment time t (min), which was described by analyzing the relative intensity of the respective absorption A_t/A_o. The net degradation was gauged by subtracting the dye removal under dark conditions. Furthermore, the photocatalytic activity mechanism was identified by trapping active species using scavengers such as isopropyl alcohol (IPA)/furfuryl alcohols (FFA), oxalate ammonium (AO), and *p*-benzoquinone (BQ) for $^{\bullet}OH$, h^+ and $^{\bullet}O_2^-$, respectively. Briefly, 1 mM of each scavenger was initiated for the TiO_2@CNF hybrid in the presence of the Rho-B dye and then kept in the photo-reactor under UVA and UVB irradiation for a duration of 3600 s. Thereafter, 3 mL of the sample was collected after 1 h intervals and centrifuged at 7000 rpm for 10 min at 20 °C.

2.6 Avobenzone compatibility

In brief, 12 μM avobenzone and 0.5 mM Brij-10 solution with 0.026 wt% Rho-B were prepared in water and the mixture was treated using ultrasound for 4 h and stored in the dark overnight. Approximately 8 mL of the reaction solution was kept in a quartz cell with continuous stirring and then placed in a photoreactor equipped with six UVA and six UVB lamps. As synthesized TiO_2 NPs and several TiO_2@CNF hybrids were tested using Avb weight ratios (Avb : TiO_2@CNF of 1 : 10, 1 : 20, 1 : 30, and 1 : 40 (w/w)). Thereafter, 3 mL of the aqueous suspension was collected every 1 h and centrifuged (7000 rpm for 10 min at 20 °C) and the maximum absorbance of avobenzone was measured at 362 nm using a UV-vis spectrometer.

2.7 Material characterization

The morphology analysis was carried out using field-emission scanning electron microscopy (FE-SEM; HITACHI S-90-X) at an accelerating voltage of 15 kV and applied current of 10 μA in the dark field mode after the sample was drop-casted on the silicon-wafer with one mint coating. Furthermore, transmission electron microscopy (TEM) images were taken with a FEI Tecnai G2 F30 microscope operated at 300 kV. The elemental composition was further analyzed by the energy dispersive X-rays spectroscopy. The electronic chemistry was characterized through X-ray photoelectron spectroscopy (XPS; ESCALAB 250Xi (Thermo Scientific) X-ray photoelectron spectrometer with monochromatic Al Kα (1486.6 eV) radiation as the excitation source). The UV shielding performance and photocatalysis activity was investigated under quartz cell with 4 mL sample by UV-vis-NIR (Cary 5000) spectroscopy. The photodegradation experiment was conducted on the UV-chamber (DYMAX-2000 model) with 48 W UVA and UVB lamps.

3. Results and discussion

3.1 Morphological analysis

Scheme 1 illustrates the preparation of the TiO_2@CNF hybrid using a simple sol–gel reaction. TiO_2 NPs were attached to the CNF surface. The morphology of the TiO_2@CNF hybrid synthesized at various concentrations was explored through transmission electron microscopy (TEM) at low and high magnification, and the results are depicted in Fig. 1(a–i). Fig. 1(a–c) reveals that the TiO_2 nanosized spherical particles were attached to the CNF surface as TiO_2@CNF1 with a TBT concentration of 0.12 wt% in the reaction solution, as shown in low and high magnifications. The TEM images display a morphology similar to that of TiO_2@CNF2 with 0.15 wt% (Fig. 1(d–f)). Under similar synthesis conditions, except for the loading amount of TiO_2 precursors for TiO_2@CNF3, a similar size (5.3 nm) was observed, and TiO_2 particles were tightly attached and homogeneously dispersed on the CNF surface even at the higher concentration of 0.19 wt% (Fig. 1(g–i)). Moreover, the surface of CNF was completely wrapped by aggregative larger-sized TiO_2 particles at the 0.24 wt% for TiO_2@CNF4, and the particle size was noted to be approximately 30 nm, as shown by the micrograph presented in ESI,

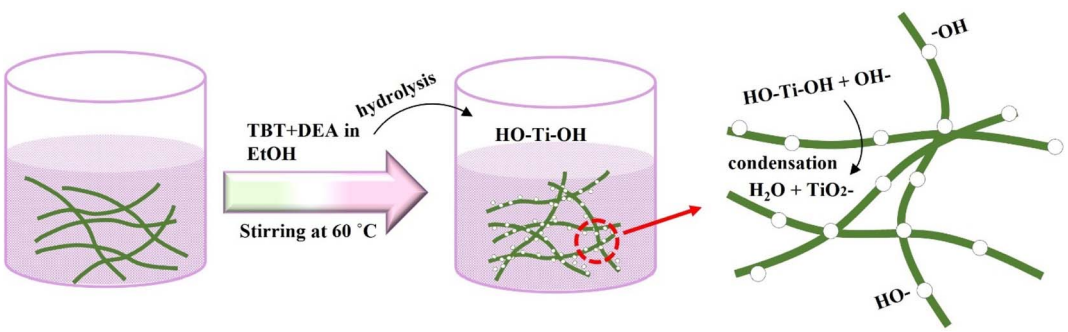

Scheme 1 Graphical illustration for the TiO_2@CNF hybrid synthesis process with derived structure.

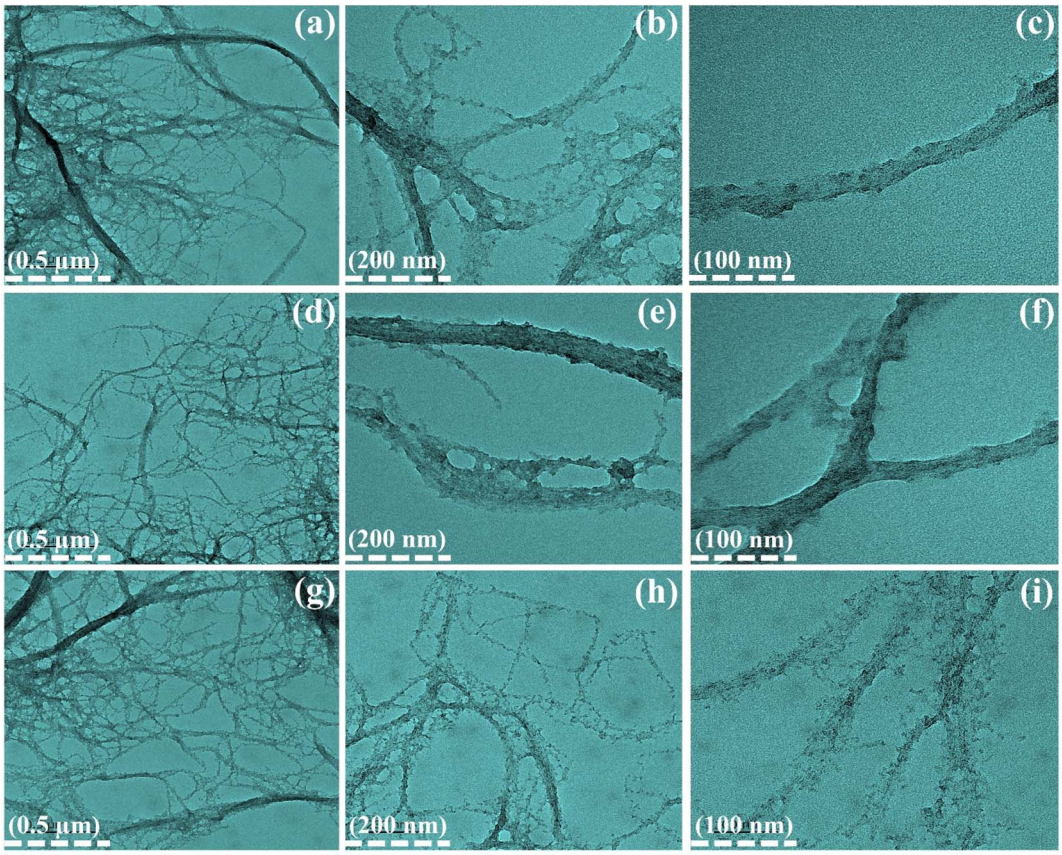

Fig. 1 Microscopic analysis of TiO_2@CNF hybrids at the various concentrations of TiO_2 NPs and pristine TiO_2 NPs: (a–c) TiO_2@CNF1 (TBT : CNF = 5 : 1), (d–f) TiO_2@CNF2 (TBT : CNF = 10 : 1), (g–i) TiO_2@CNF3 (TBT : CNF = 15 : 1).

S6.† TiO_2 without CNF showed an aggregative-like morphology and an approximate 27 nm of size was observed (ESI, S7†).

Energy dispersive X-ray (EDX) analysis was carried out to detect elements, their wt%, and their composition; the results are illustrated in Fig. 2(a–c). The EDX spectrum of TiO_2@CNF1–3 confirmed the presence of three elements, carbon (C), oxygen (O), and titanium (Ti), respectively. A higher weight percentage of Ti was observed for the TiO_2@CNF3 hybrid, owing to the higher precursor amount. The amounts (%) of these three elements were found to be 34.36, 33.36, and 32.36% for C; 45.6, 42.6, and 37.40% for O; and 20.04, 24.04, and 30.24% of Ti were obtained from TiO_2@CNF1, TiO_2@CNF2, and TiO_2@CNF3, respectively, implying an excellent composition. Furthermore, the yield of TiO_2 was determined by calcination of the sample, where the as-prepared sample in triplicate aluminum dishes was completely dried in an oven and then placed in a furnace at 250 °C for approximately 30 min and then at 500 °C for 2 h. The yield was 78% for the TBT concentration of 0.19 wt%, which is close to that of TiO_2 synthesized without CNF (pristine TiO_2) of 85%. At 0.12 wt% and 0.15 wt%, the yield was obtained by 65% and 70%, respectively, which is a significant value for application in the field of cosmetics, especially sunblock products (Fig. 2d).

Furthermore, the valence states and chemical composition of the pristine TiO_2 and optimized TiO_2@CNF3 hybrid were studied using X-ray photoelectron spectroscopy (XPS) measurements. Fig. 3(a) shows the survey spectra of the pristine TiO_2 and TiO_2@CNF3 hybrid, demonstrating all the peaks of C 1s, O 1s, and Ti 2p. Fig. 3(b and d) show the Ti 2p element binding energy XPS profile with an intense symmetrical doublet at 459.8 eV and 465.4 eV, owing to Ti $2p_{3/2}$ and Ti $2p_{1/2}$, for pristine TiO_2 and TiO_2@CNF3 hybrid, respectively.[26,27] The peak positions and difference of energy ΔE values between Ti $2p_{1/2}$ and Ti $2p_{3/2}$ was approximately 5.6 eV, demonstrating that the element of Ti in TiO_2@CNF3 hybrid is mainly Ti^{4+}.[28] The main peaks at 530.8 eV and 530.9 eV in the O 1s XPS profile can be ascribed to the O in the form of the O–Ti bond, whereas the peak positioned at 532.0 eV can be ascribed to the H–O from the absorbed water on the surface.[29,30] These results are illustrated in Fig. 3(c and e). For the C 1s XPS profile shown in Fig. 3(f), XPS spectra exposes the three peaks at 284.6 eV, 285.5 eV, and 286.2 eV, which can be ascribed to the C–C natural bond, C–O, and O–C–O.[31] Based on these results, it was concluded that TiO_2 was successfully synthesized on the CNF surfaces.

3.2 UV shielding performance of TiO_2@CNF hybrids

The UV-shielding performance of the TiO_2@CNF hybrids was further validated using a UV-vis spectrophotometer. Fig. 4(a) shows the enhancement in the UV absorption of the TiO_2@CNF hybrid with increasing amounts of TiO_2 precursors at 220–

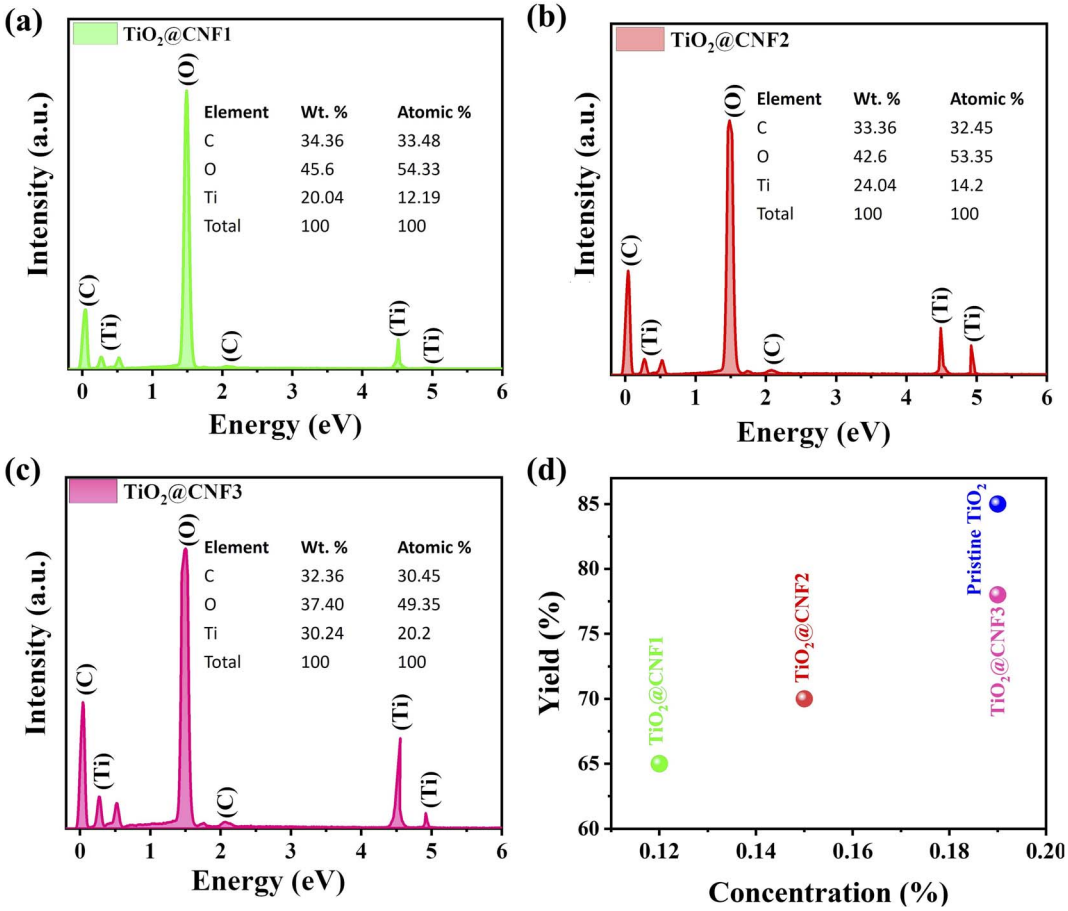

Fig. 2 EDX analysis for TiO_2@CNF hybrids at the various concentrations of TiO_2 NPs and pristine TiO_2 NPs: (a) TiO_2@CNF1, (b) TiO_2@CNF2, (c) TiO_2@CNF3 and (d) the yield (%) of TiO_2 in terms of TBT concentration.

400 nm. The UV absorption drastically increases at 0.12 wt%, 0.15 wt%, and 0.19 wt%, after which the enhancement becomes insignificant at the 0.24 wt% of concentration. The phenomena can be explained as follows: the TiO_2 NPs are attached uniformly to the CNF surface at the 0.12–0.19 wt% of concentration (good dispersion), the UV absorption is drastically enhanced, and the results are comparable to the previous reports.[12,15,32] Once the surface of the CNF was completely blocked by TiO_2 NPs, the UV enhancement decreased owing to the high aggregation. When the TiO_2 NPs with a size of 30 nm were incorporated with CNF, the TiO_2@CNF4 hybrid was able to block the UV radiation at 220–400 nm, and the visible light transparency reduced by 40%. UV light below 400 nm was efficiently blocked, whereas the visible light transparency was still high, which is further illustrated in Fig. 4(b) at wavelengths of 220 nm and 800 nm. The UV absorption of the pristine TiO_2 NPs was significantly lower than that of the other hybrid samples. This indicates a larger particle size (approximately 27 nm) and an aggregative-like structure. It is well known that aggregative particles scatter more visible light and deteriorate the transparency.[33]

Interestingly, the TiO_2@CNF4 hybrid exhibited a higher UV absorption performance than pristine TiO_2, even though the size of the TiO_2 NPs was larger, demonstrating the CNF effect in the hybrid product. Additionally, the CNF without TiO_2 NPs can also absorb UV light, as shown in Fig. 4(a). Generally, the UV-shielding performance of nanosized particles can be ascribed to scattering and absorption.[34,35] Thus, the UV shielding performance of TiO_2-based NPs mainly depends on the absorbed energy and scattering effect on light, which are correlated with the particle size, morphology, and intrinsic properties of the samples. Because the particle size and morphology of the three TiO_2@CNF1–3 hybrid nanostructures are similar, their scattering effect on light may be similar. Therefore, the difference in UV absorption may be due to the intrinsic optical properties of the TiO_2 NPs.

A dispersion stability test was performed in DI water. As shown in Fig. 4(c), pristine TiO_2 NPs in DI water cannot be stabilized for a long time at lower and higher concentrations, whereas the hybrid nanostructures show stable dispersion in water owing to the hydrophilic nature of CNF (CNF was used as a binder polymer). The dispersion stability mechanism can be ascribed to the depletion force in terms of nanoparticle size and polymer dimensions.[36] It is well accepted that longer polymer dimensions may promote strong and long-range depletion interactions between NPs.[37] In this scenario, CNF may trigger a strong interaction at a greater distance between the TiO_2 NPs and prevent aggregation.

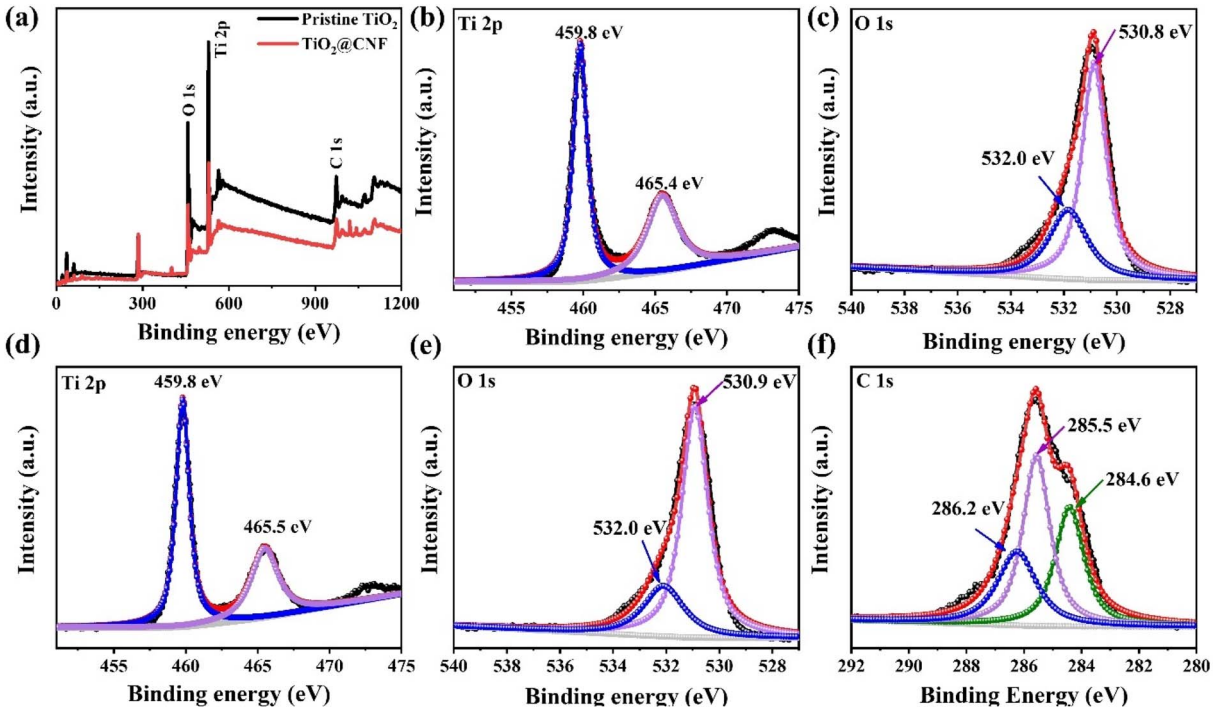

Fig. 3 (a) XPS survey spectrum of the pristine TiO_2 and optimized TiO_2@CNF3 hybrid, (b) high-resolution XPS spectrum of the Ti 2p for pristine TiO_2 (c) high-resolution XPS spectrum of the O 1s for pristine TiO_2, (d) high-resolution XPS spectrum of the Ti 2p for TiO_2@CNF3, (e) high-resolution XPS spectrum of the O 1s for TiO_2@CNF3 and (f) high-resolution XPS spectrum of C 1s for TiO_2@CNF3.

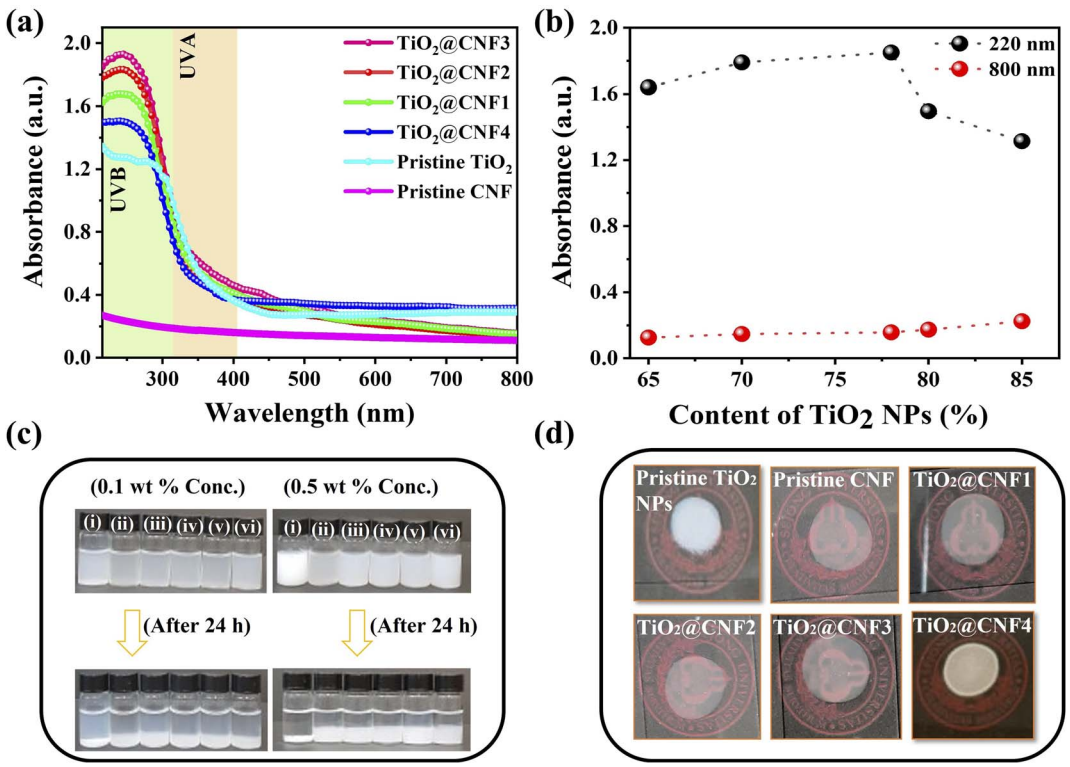

Fig. 4 UV shielding performance for the (a) pristine TiO_2 NPs, TiO_2@CNF4, TiO_2@CNF3, TiO_2@CNF2, TiO_2@CNF1 hybrids and pristine CNF, and (b) summary of the UV absorption at the 220 nm and 800 nm of wavelength. (c) Dispersion effect at the 0.1 wt% and 0.5 wt% of concentrations after 0 h and 24 h such as (i) pristine TiO_2 NPs, (ii) pristine CNF, (iii) TiO_2@CNF1, (iv) TiO_2@CNF2, (v) TiO_2@CNF3 and (vi) TiO_2@CNF4. (d) Photo digital images for all samples to assess the whitening effect.

A drop-casting method was employed to further investigate the whitening effect of the products. It is well known that pristine TiO_2 shows a whiter chalk-like layer when applied to the skin. As can be seen in the digital image in Fig. 4(d), the TiO_2@CNF1–3 hybrid suppresses the whitening effect due to the incorporation of hydrophilic CNF, whereas the pristine TiO_2 and TiO_2@CNF4 hybrid show a white color, which is mainly due to the larger size of particles as well as aggregations. This proves that TiO_2-based CNF as a hybrid product can be used in cosmetics for skincare formulations because of the hydrophilic CNF, which means that these particles are effectively soluble in water (enhancing the dispersion stability).

3.3 Photocompatibility of avobenzone with the TiO_2@CNF hybrid

The photocompatibility of UV-shielding materials is of great importance for their practical application in cosmetics. An organic UV absorber, avobenzone (Avb), was illuminated under UVA and UVB radiation in a solution of TiO_2-based NPs. Avb as a sunblock ingredient can shield the skin from UVA radiation, which is largely present in an enol form that can photodegrade under UVA–UVB exposure through a photo-induced enol–keto transformation mechanism.[38] Various sunblock products can be stabilized either by quenching the excited states or by competitive light absorption. As avobenzone is widely used as a sunblock ingredient, it is important to develop compatibility with the new nanosized particles to evaluate the extent to which it can be involved in the photodegradation of Avb.

Fig. 5(a–h) show the photodegradation of avobenzone after UVA and UVB illumination for 300 min with several TiO_2@CNF concentrations (0.12, 0.15, and 0.19 wt%). Approximately 6–7% degradation of Avb was obtained under UVA and UVB illumination with the TiO_2@CNF1 hybrid (0.12 wt%) at 362 nm, respectively. When the concentration was increased to 0.15 wt%, with ~13 and ~8%, photodegradation were detected

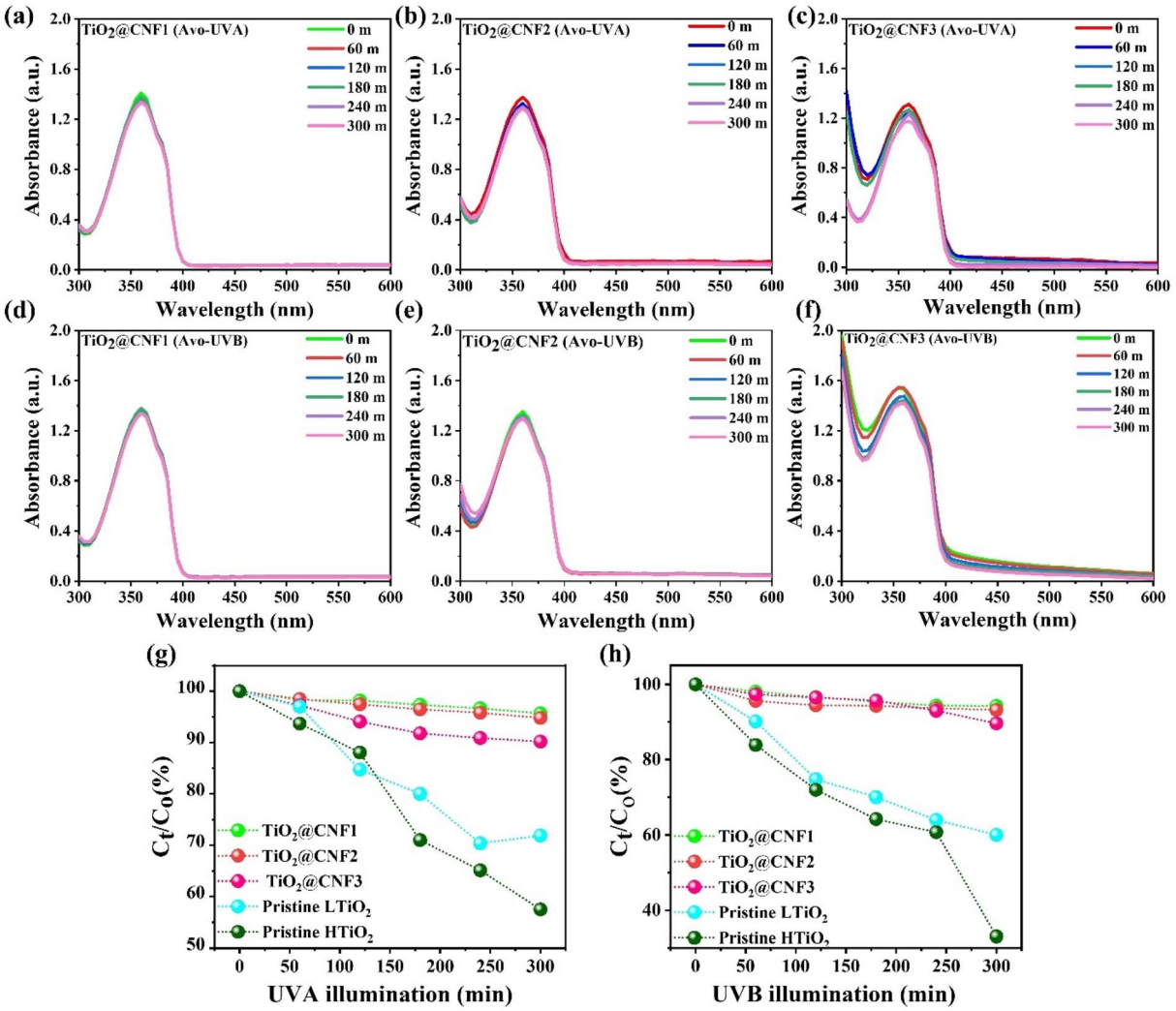

Fig. 5 Avobenzone (Avb) compatibility with TiO_2@CNF hybrid at the low and high concentrations under UVA and UVB illuminations for 300 min, respectively, (a–c) TiO_2@CNF1, TiO_2@CNF2 and TiO_2@CNF3 hybrid with Avb (0.2 μg L^{-1}) under UVA, respectively. (d–f) TiO_2@CNF1, TiO_2@CNF2 and TiO_2@CNF3 hybrid with Avb (0.2 μg L^{-1}) under UVB, respectively. (g and h) Degradation efficiency (%) with respect to the UVA and UVB illuminations, respectively. Notice: $LTiO_2$, $HTiO_2$ means the lower and higher concentration of the TiO_2 NPs.

under UVA and UVB illumination, respectively. More importantly, the Avb absorption spectral intensity gradually decreased after exposure to UVA/UVB illumination at a 0.19 wt% of concentration. More than 80% photoprotection was observed even at the higher concentrations of the TiO_2 NPs on CNF under UVA and UVB illumination. Pristine TiO_2 NPs were also examined for photoprotection under the same conditions (ESI, S8–S11†). It is shown that ~40, 36.1% and 60, 54% degradation of Avb was obtained in the presence of TiO_2 without CNF under UVA and UVB illumination, respectively, demonstrating that the TiO_2 NPs do not have the ability to retain the photoprotection with avobenzone (Fig. 5(g and h)). The photoprotection of the pristine Avb (the same concentration) in water was also examined with UVA and UVB illumination for approximately 300 m. Approximately 30% and 21% Avb spectrum was degraded with the initial spectrum of Avb with UVA and UVB illumination, respectively, which indicated that pristine Avb does not have enough stability under UVA and UVB illumination (ESI, S12 & S13†). It is interesting to note the excellent photoprotection of the new hybrid TiO_2@CNF even at a higher concentration of TiO_2 NPs on CNF, suggesting good compatibility with Avb.

3.4 Transmittance performance of the modified commercial sunblock's with CNF

Generally, commercial sunblock products are categorized into two categories based on their active ingredients: inorganic and organic. Both commercial inorganic and organic sunblock products with SPF lifetimes of 35^+ and 50^+ were mixed with CNF, and their transmittance performance was investigated.

Fig. 6(a and b) shows the transmittance spectra of inorganic sunblock products mixed with CNF gel (2 wt%) at 0.1 and 0.2 mg mL^{-1}. After the addition of 3 g CNF gel to ioSB1 (SPF 35^+), the transmittance was dramatically enhanced by ~43% at 0.1 mg mL^{-1} in the visible region, and by ~52% in the case of 5 g CNF gel addition, as seen in Fig. 6(a). For ioSB2 (SPF 50^+), transmittance increased by ~13 and 24% after the addition of 3 and 5 g of CNF gel compared to that of without CNF, respectively, as shown in Fig. 6(b). When the amount of sunblock was increased from 0.1 to 0.2 mg mL^{-1}, the transmittance decreases.

Similar effects were observed for organic sunblock products oSB1 (SPF 50^+) and oSB2 (SPF 50^+). For oSB1, transmittance increased by ~25% and ~32% after the addition of 3 g and 5 g CNF gel, respectively, in the visible region at 0.1 mg mL^{-1}, as

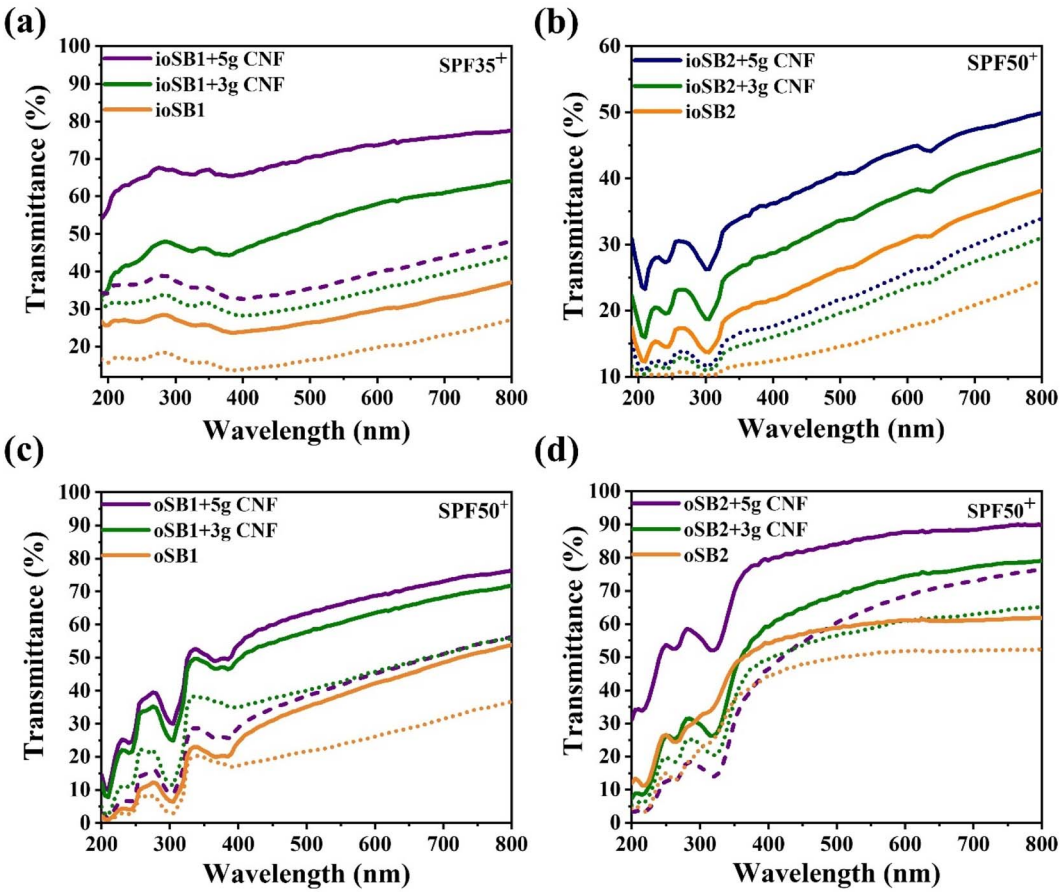

Fig. 6 Transmittance performance of the commercial inorganic and organic sunblock's with SPF life 35^+ and 50^+ containing different CNF amounts in the 200–800 nm of wavelength ranging. The corresponding SPF 35^+ and 50^+ sunblocks (ioSB1 and ioSB2 are inorganic while oSB1 and oSB2 are organic sunblocks) were purchased by the multiple companies and used as a reference. (a) HERA sun mate daily cream; modified by the CNF (ioSB1(35^+) + 3 and 5 g CNF gel), (b) the face shop natural sun block eco super perfect with SPF life 50^+; modified by CNF *i.e.*, ioSB2(50^+) + CNF gel with 3 and 5 g (c) MediFlower brand sunblock; modified by CNF (oSB1(50^+) + CNF with 3 and 5 g) (d) V10 UV shield; modified by CNF (oSB2(50^+) + CNF with 3 and 5 g). Solid and dotted lines indicate 0.1 and 0.2 mg mL^{-1}, respectively.

shown in Fig. 6(c). For oSB2, transmittance increased by ~20% and ~33% after the addition of 3 g and 5 g CNF gel, respectively, as shown in Fig. 6(d).

A further increase in the amount of CNF in the sunblock products did not improve the transmittance of either inorganic or organic sunblock. Although the underlying mechanism remains to be elucidated, transmittance enhancement through CNF may be related to improved dispersion of sunblock active ingredients as well as enhanced emulsion stability by CNF.[39,40]

In addition, the whitening effect of these CNF-based sunblock products at high and low concentrations was investigated; the results are illustrated ESI, S14.† The pure sunblock products, ioSB1(35^+), ioSB2(50^+), oSB1(50^+), and oSB2(50^+), clearly show a white color compared to the sunblock products mixed with CNF. Therefore, it is indicated that CNF can decrease the whitening effect and increase the transmittance effect.

3.5 Photodegradation test using Rho-B

It is well known that reduction kinetics can be examined through spectroscopic measurements based on the color changes that participate in photocatalysis reactions.[27,41,42] Rho-B absorption spectra at 555 nm wavelength showed negligible absorption over the UVA and UVB illuminations for 300 min (ESI, S15 & S16†). The TiO_2@CNF1, TiO_2@CNF2, and TiO_2@-CNF3 hybrids and pristine TiO_2 NPs were added to the Rho-B solution, and the corresponding spectra under UVA illumination are shown in ESI, S17–S20.† Approximately 8.7, 12, and 14.8% of Rho-B degradation occurred, and the results are presented in Fig. 7(a). It is inferred that the degradation rate of Rho-B for TiO_2@CNF3 is slightly increased owing to the higher concentration of the TiO_2 precursors, that is, 0.19 wt%. A rapid decomposition of the Rho-B in the solution of the pristine TiO_2 NPs was observed, and more than 95% of Rho-B was decomposed after 240 min of UVA illumination, indicating higher photocatalytic performance of the pristine TiO_2 NPs. UVB irradiation was also applied to TiO_2 modified with the hybrid at different concentrations and pristine TiO_2 NPs for 300 min (S21–S24†). The degradation results were similar to those of UVA illumination, as shown in Fig. 7(b).

Few researchers have used the coating method to reduce the photocatalytic activity of TiO_2 particles using SiO_2, silica, and Al_2O_3,[15,16,43,44] where the core–shell structure is formed. Even

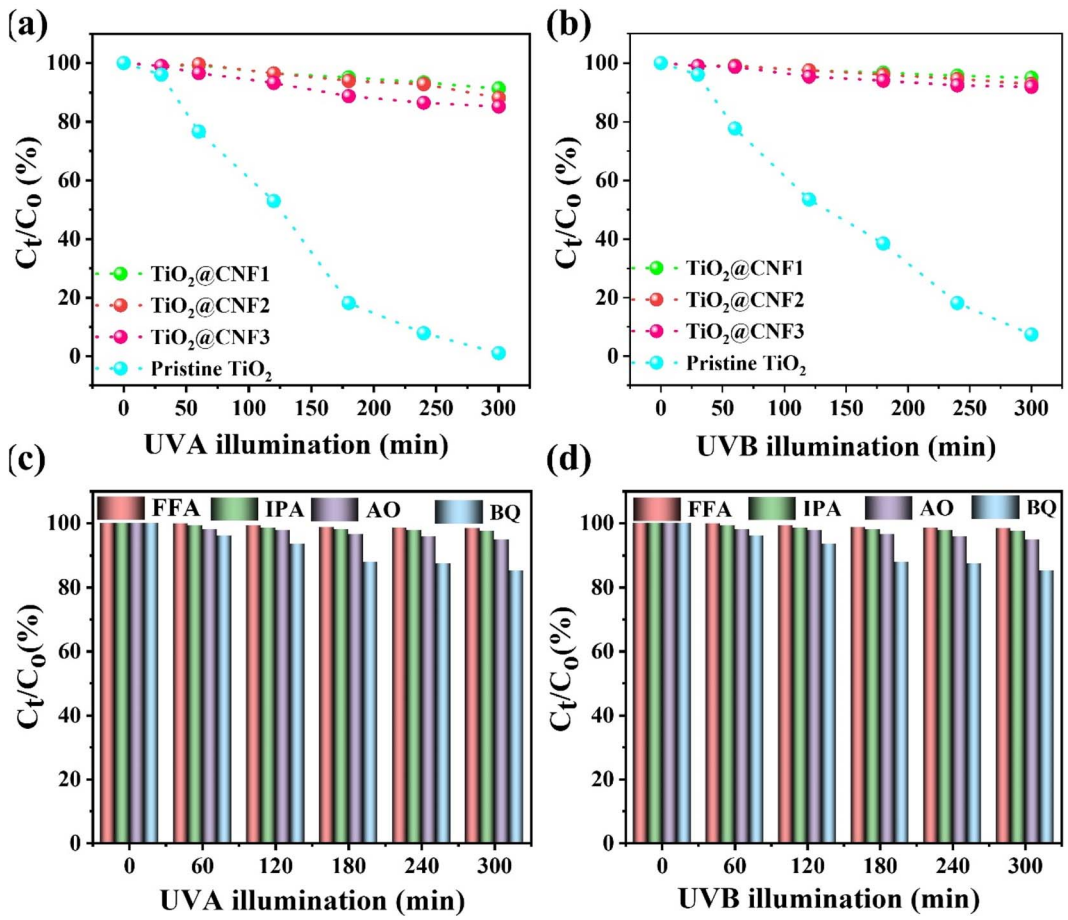

Fig. 7 Photocatalysis activity of the TiO_2@CNF1–3 hybrids and pristine TiO_2 NPs. (a and b) Change of Rho-B concentration against UVA and UVB illumination time, respectively and (c and d) change of Rho-B concentration against UVA and UVB illumination time using various scavengers such as FFA, IPA, AO and BQ, respectively.

Table 1 TiO_2@CNF hybrid with the outcomes

Experiment name	UV-blocking performance	Photocatalysis activity	Photocompatibility of the AVB	Yield of the TiO_2 on CNF
TiO_2@CNF1	1.64 a.u. in UV region	8.7% Rho-B dye degraded	6–7% under UVA and UVB	0.12 wt% (65% productivity)
TiO_2@CNF2	1.78 a.u. in UV region	12% Rho-B dye degraded	13 & 7% under UVA and UVB	0.15 wt% (70% productivity)
TiO_2@CNF3	1.85 a.u. in UV region	14.8% Rho-B dye degraded	About 20% under UVA and UVB	0.19 wt% (78% productivity)
TiO_2	1.34 a.u. absorbance	95% Rho-B dye degraded	60 & 40% under UVA and UVB	0.19 wt% (85% productivity)

Table 2 Compared studies with previous researchers for the investigation of photocatalysis property under different conditions

Experiment name	Illumination/time (min)	Reduction in degradation%	Dyes	Ref.
TiO_2@CNF3	UV lamp/300	14.8	Rho-B	Present work
Pristine TiO_2	UV lamp/300	95	Rho-B	Present work
Silica–ZnO	Xenon lam/100	39	Rho-B	47
Silica–ZnO	Xenon lamp/100	42	MB	48
Silica–ZnO	Xenon lamp/150	45.9	Rho-B	49
PVP–silica@ZnO	Xenon lamp/120	45.4	Rho-B	50
PVP-capped ZnO	—	36.6	Rho-B	51
2 : 1 CHI/TiO_2	UV lamp/120	60.5	CV	52
2 : 1 CHI/TiO_2	UV lamp/120	41.7	CV	52
TiO_2@Y_2O_3(10 wt%)	UV lamp/30	36.4	CV	53
TiO_2@Y_2O_3(5 wt%)	UV lamp/30	47.5	CV	53
Sg1 and SV1	Xenon lamp/30	40–30	Rho-B	54
6 wt% Mn–ZnO	UV lamp/210	36	MB	55
2 wt% Mn–ZnO	UV lamp/210	47	MB	55

though the photocatalytic activity of TiO_2 was suppressed, the UV shielding performance was not enhanced. Therefore, the attachment of nanosized TiO_2 particles on the CNF surface could remove this challenge, and the TiO_2@CNF hybrid exhibited a higher UV shielding performance as well as abridged photocatalytic activity. The detail experimental performance about the TiO_2@CNF with outcomes are shown in Table 1 and the photocatalysis activity comparison performance was shown in Table 2. These attributes are strongly suggested in the field of cosmetics owing to their safe and effective usage of sunblock on a global scale.

Furthermore, to understand the mechanism of the photocatalytic activity, radical quenching was employed. Scavengers, that is, IPA/FFA, AO, and BQ, were used to quench ROS such as $^{\bullet}OH$, h^+ and $^{\bullet}O_2^-$, respectively, under UVA and UVB illumination, as shown in Fig. 7(c and d).[27,45,46] For TiO_2@CNF3, only ~2.24, 3.01% and 1.34, 1.98% of Rho-B degradation have been observed in the presence of the IPA and FFA, demonstrating that these scavengers controlled the $^{\bullet}OH$ reactive radical species. It is indicated that the degradation is observed in hybrid experiments in the order of photocatalytic oxidation (PCO), owing to the repeated attacks of the $^{\bullet}OH$ radicals in the photocatalyst experiment. Briefly, the three scavengers can be quenched in the sequence: IPA/FFA > AO > BQ, indicating that ROS plays a major role in the degradation of Rho-B rather than that of h^+ under UVA and UVB illumination. Based on these results, it can be concluded that $^{\bullet}OH$ is the most important reactive species in the TiO_2@CNF3 catalyzed PCO path of Rho-B.

4. Conclusion

A simple and cost-effective sol–gel strategy was used to synthesize TiO_2 NPs on CNF as a TiO_2@CNF hybrid. The hybrid exhibited an excellent UV-blocking effect owing to the uniformly dispersed nanosized particles on the surface of the CNF. The photocompatibility of the hybrid with the avobenzone particles was also investigated. It is interesting to note that more than 80% photoprotection was observed with the hybrid under UVA and UVB illumination at higher concentrations for 300 min than that of pristine TiO_2 NPs (<60%), thus indicating excellent photostability. Furthermore, the TiO_2 photocatalytic activity was examined from a cosmetic perspective. Less than 20% of Rho-B dye was degraded through the POC process during hybridization at higher content of the TiO_2 after exposure to UVA and UVB illumination for 300 min, respectively, than that of pristine TiO_2 NPs (more than 95%), suggesting a safe and effective TiO_2-incorporated CNF photoprotector. CNF was further employed in commercial inorganic and organic sunblock products with SPF lifetimes of 35^+ and 50^+, respectively, owing to the above-mentioned versatile attributes. The transmittance effect of the inorganic sunblock products ioSB1 and ioSB2 (with SPF lifetimes of 35^+ and 50^+) increased by 52 and 24%, whereas that of the organic sunblock products oSB1 and oSB2 (with SPF life 50^+) increased by 32 and 33% with of 5 g CNF gel, respectively. This was attributed to the synergistic effect of CNF and other active ingredients in the sunblock, as well as the hydrophilic nature of CNF. This study demonstrated the potential of CNF with other active ingredients in value-added cosmetics.

Conflicts of interest

The authors declare that they have no known competing financial interests or personal relationships that could have appeared to influence the work reported in this paper.

Abbreviations

CNF	Cellulose nanofiber
TiO_2	Titanium dioxide
DEA	Diethanolamine
TBT	Titanium tetra-*n*-butoxide
Avb	Avobenzone
ioSB1	Inorganic sunblock 35^+
ioSB2	Inorganic sunblock 50^+
oSB1 and oSB2	Organic sunblock 50^+
UVA	Ultraviolet-A
UVB	Ultraviolet-B
Rho-B	Rhodamine-B
MB	Methylene B
FFA	Furfuryl alcohol
AO	Ammonium oxalate
BQ	*p*-Benzoquinone
IPA	Isopropyl alcohol
ROS	Reactive oxygen species

Acknowledgements

This research was supported by R&D Program for Forest Science Technology (FTIS2020214D10-2022-AC01) provided Korean Forest Service (Korean Forestry Promotion Institute), Basic Research Laboratory Program (2021R1A4A5033289) through the National Research Foundation of Korea (NRF) funded by the Ministry of Education and the Technology Innovation Program and the Technology Innovation Program (20017464) funded by the Ministry of Trade, Industry & Energy (MOTIE, Korea).

References

1 R. Dickerson, S. Kondragunta, G. Stenchikov, K. Civerolo, B. Doddridge and B. Holben, The impact of aerosols on solar ultraviolet radiation and photochemical smog, *Science*, 1997, **278**(5339), 827–830.

2 Y. Wang, C. Xiang, T. Li, P. Ma, H. Bai, Y. Xie, M. Chen and W. Dong, Enhanced thermal stability and UV-shielding properties of poly(vinyl alcohol) based on Esculetin, *J. Phys. Chem. B*, 2017, **121**(5), 1148–1157.

3 M. Zayat, P. Garcia-Parejo and D. Levy, Preventing UV-light damage of light sensitive materials using a highly protective UV-absorbing coating, *Chem. Soc. Rev.*, 2007, **36**(8), 1270–1281.

4 Y. Wang, T. Li, P. Ma, H. Bai, Y. Xie, M. Chen and W. Dong, Simultaneous enhancements of UV-shielding properties and photostability of poly(vinyl alcohol) *via* incorporation of *Sepia eumelanin*, *ACS Sustainable Chem. Eng.*, 2016, **4**(4), 2252–2258.

5 Y. Wang, Z. Mo, C. Zhang, P. Zhang, R. Guo, H. Gou, R. Hu and X. Wei, Morphology-controllable 3D flower-like TiO_2 for UV shielding application, *J. Ind. Eng. Chem.*, 2015, **32**, 172–177.

6 K.-Q. Liu, C.-X. Kuang, M.-Q. Zhong, Y.-Q. Shi and F. Chen, Synthesis, characterization and UV-shielding property of polystyrene-embedded CeO_2 nanoparticles, *Opt. Mater.*, 2013, **35**(12), 2710–2715.

7 V. Augugliaro, M. Bellardita, V. Loddo, G. Palmisano, L. Palmisano and S. Yurdakal, Overview on oxidation mechanisms of organic compounds by TiO_2 in heterogeneous photocatalysis, *J. Photochem. Photobiol., C*, 2012, **13**(3), 224–245.

8 M. A. Fox and M. T. Dulay, Heterogeneous photocatalysis, *Chem. Rev.*, 1993, **93**(1), 341–357.

9 B. Gulson, M. McCall, M. Korsch, L. Gomez, P. Casey, Y. Oytam, A. Taylor, M. McCulloch, J. Trotter and L. Kinsley, Small amounts of zinc from zinc oxide particles in sunscreens applied outdoors are absorbed through human skin, *Toxicol. Sci.*, 2010, **118**(1), 140–149.

10 X. Deng, Q. Luan, W. Chen, Y. Wang, M. Wu, H. Zhang and Z. Jiao, Nanosized zinc oxide particles induce neural stem cell apoptosis, *Nanotechnology*, 2009, **20**(11), 115101.

11 S. Afonso, K. Horita, J. S. e Silva, I. Almeida, M. Amaral, P. Lobão, P. Costa, M. S. Miranda, J. C. E. da Silva and J. S. Lobo, Photodegradation of avobenzone: stabilization effect of antioxidants, *J. Photochem. Photobiol., B*, 2014, **140**, 36–40.

12 H. Ju, Y. Jiang, B. Xue, Y. Xu, H. Guo, M. Huo and F. Li, UV shielding performance of illite/TiO_2 nanocomposites, *New J. Chem.*, 2018, **42**(11), 9260–9268.

13 J. Huang, S. Li, M. Ge, L. Wang, T. Xing, G. Chen, X. Liu, S. S. Al-Deyab, K. Zhang and T. Chen, Robust superhydrophobic TiO_2@fabrics for UV shielding, self-cleaning and oil–water separation, *J. Mater. Chem. A*, 2015, **3**(6), 2825–2832.

14 Y. Li, D. Yang, S. Lu, X. Qiu, Y. Qian and P. Li, Encapsulating TiO_2 in lignin-based colloidal spheres for high sunscreen performance and weak photocatalytic activity, *ACS Sustainable Chem. Eng.*, 2019, **7**(6), 6234–6242.

15 Y. Bai, Z. Li, B. Cheng, M. Zhang and K. Su, Higher UV-shielding ability and lower photocatalytic activity of TiO_2@SiO_2/APTES and its excellent performance in enhancing the photostability of poly(*p*-phenylene sulfide), *RSC Adv.*, 2017, **7**(35), 21758–21767.

16 A. M. El-Toni, S. Yin, T. Sato, T. Ghannam, M. Al-Hoshan and M. Al-Salhi, Investigation of photocatalytic activity and UV-shielding properties for silica coated titania nanoparticles by solvothermal coating, *J. Alloys Compd.*, 2010, **508**(1), L1–L4.

17 J. Du and H. Sun, Polymer/TiO_2 hybrid vesicles for excellent UV screening and effective encapsulation of antioxidant agents, *ACS Appl. Mater. Interfaces*, 2014, **6**(16), 13535–13541.

18 S. Yamada, E. Mouri and K. Yoshinaga, Incorporation of titanium dioxide particles into polymer matrix using block

copolymer micelles for fabrication of high refractive and transparent organic–inorganic hybrid materials, *J. Polym. Sci., Part A: Polym. Chem.*, 2011, **49**(3), 712–718.

19 B. G. Chiari, E. Trovatti, É. Pecoraro, M. A. Corrêa, R. M. B. Cicarelli, S. J. L. Ribeiro and V. L. B. Isaac, Synergistic effect of green coffee oil and synthetic sunscreen for health care application, *Ind. Crops Prod.*, 2014, **52**, 389–393.

20 P. N. Shenekar, P. S. Ukirade, S. D. Salunkhe, S. T. Sutar, C. Magdum, S. Mohite, S. G. Lokapure and S. M. Metri, *In vitro* evaluation of sun protection factor of fruit extract of *Carica papaya* L. as a lotion formulation, *Eur. J. Exp. Biol.*, 2014, **4**(2), 44–47.

21 P. P. Maske, S. G. Lokapure, D. Nimbalkar, S. Malavi and J. I. D'souza, In vitro determination of sun protection factor and chemical stability of *Rosa kordesii* extract gel, *J. Pharm. Res.*, 2013, **7**(6), 520–524.

22 A. Jarzycka, A. Lewińska, R. Gancarz and K. A. Wilk, Assessment of extracts of *Helichrysum arenarium*, *Crataegus monogyna*, *Sambucus nigra* in photoprotective UVA and UVB; photostability in cosmetic emulsions, *J. Photochem. Photobiol., B*, 2013, **128**, 50–57.

23 Y. Li, Y. Liu, Y. Liu, W. Lai, F. Huang, A. Ou, R. Qin, X. Liu and X. Wang, Ester crosslinking enhanced hydrophilic cellulose nanofibrils aerogel, *ACS Sustainable Chem. Eng.*, 2018, **6**(9), 11979–11988.

24 I. Rabani, J. Yoo, H.-S. Kim, S. Hussain, K. Karuppasamy and Y.-S. Seo, Highly dispersive Co_3O_4 nanoparticles incorporated into a cellulose nanofiber for a high-performance flexible supercapacitor, *Nanoscale*, 2021, **13**(1), 355–370.

25 M. Catauro, E. Tranquillo, G. Dal Poggetto, M. Pasquali, A. Dell'Era and S. Vecchio Ciprioti, Influence of the heat treatment on the particles size and on the crystalline phase of TiO_2 synthesized by the sol–gel method, *Materials*, 2018, **11**(12), 2364.

26 Y. Chen, L. Du, P. Yang, P. Sun, X. Yu and W. Mai, Significantly enhanced robustness and electrochemical performance of flexible carbon nanotube-based supercapacitors by electrodepositing polypyrrole, *J. Power Sources*, 2015, **287**, 68–74.

27 I. Rabani, C. Bathula, R. Zafar, G. Z. Rabani, S. Hussain, S. A. Patil and Y. S. Seo, Morphologically engineered metal oxides for the enhanced removal of multiple pollutants from water with degradation mechanism, *J. Environ. Chem. Eng.*, 2021, **9**(1), 104852.

28 Z. Song, J. Hrbek and R. Osgood, Formation of TiO_2 nanoparticles by reactive-layer-assisted deposition and characterization by XPS and STM, *Nano Lett.*, 2005, **5**(7), 1327–1332.

29 S. S. Mali, C. A. Betty, P. N. Bhosale and P. Patil, Synthesis, characterization of hydrothermally grown MWCNT–TiO_2 photoelectrodes and their visible light absorption properties, *ECS J. Solid State Sci. Technol.*, 2012, **1**(2), M15.

30 C. C. Chen, Y. P. Fu and S. H. Hu, Characterizations of TiO_2/SiO_2/Ni–Cu–Zn ferrite composite for magnetic photocatalysts, *J. Am. Ceram. Soc.*, 2015, **98**(9), 2803–2811.

31 J. Liu, Q. Zhang, J. Yang, H. Ma, M. O. Tade, S. Wang and J. Liu, Facile synthesis of carbon-doped mesoporous anatase TiO_2 for the enhanced visible-light driven photocatalysis, *Chem. Commun.*, 2014, **50**(90), 13971–13974.

32 Y. Kim, J. Suhr, H.-W. Seo, H. Sun, S. Kim, I.-K. Park, S.-H. Kim, Y. Lee, K.-J. Kim and J.-D. Nam, All biomass and UV protective composite composed of compatibilized lignin and poly(lactic-acid), *Sci. Rep.*, 2017, **7**(1), 1–11.

33 Y. Wang, X. Wang, T. Li, P. Ma, S. Zhang, M. Du, W. Dong, Y. Xie and M. Chen, Effects of melanin on optical behavior of polymer: from natural pigment to materials applications, *ACS Appl. Mater. Interfaces*, 2018, **10**(15), 13100–13106.

34 P. Chýlekt, Light scattering by small particles in an absorbing medium, *JOSA*, 1977, **67**(4), 561–563.

35 X. Xue, P. Deng, B. He, Y. Nie, L. Xing, Y. Zhang and Z. L. Wang, Flexible self-charging power cell for one-step energy conversion and storage, *Adv. Energy Mater.*, 2014, **4**(5), 1301329.

36 D. Ray, V. Aswal and J. Kohlbrecher, Micelle-induced depletion interaction and resultant structure in charged colloidal nanoparticle system, *J. Appl. Phys.*, 2015, **117**(16), 164310.

37 R. Tuinier and H. N. Lekkerkerker, *Colloids and the Depletion Interaction*, Springer Netherlands, 2011.

38 Z. Chen, W. Wang, Z. Zhang and X. Fang, High-efficiency visible-light-driven Ag_3PO_4/AgI photocatalysts: Z-scheme photocatalytic mechanism for their enhanced photocatalytic activity, *J. Phys. Chem. C*, 2013, **117**(38), 19346–19352.

39 I. Rabani, S.-H. Lee, H.-S. Kim, J. Yoo, Y.-R. Park, T. Maqbool, C. Bathula, Y. Jamil, S. Hussain and Y.-S. Seo, Suppressed photocatalytic activity of ZnO based Core@Shell and RCore@Shell nanostructure incorporated in the cellulose nanofiber, *Chemosphere*, 2021, **269**, 129311.

40 I. Rabani, S.-H. Lee, H.-S. Kim, J. Yoo, S. Hussain, T. Maqbool and Y.-S. Seo, Engineering-safer-by design ZnO nanoparticles incorporated cellulose nanofiber hybrid for high UV protection and low photocatalytic activity with mechanism, *J. Environ. Chem. Eng.*, 2021, **9**(5), 105845.

41 S. Tang, S. Vongehr and X. Meng, Controllable incorporation of Ag and Ag–Au nanoparticles in carbon spheres for tunable optical and catalytic properties, *J. Mater. Chem.*, 2010, **20**(26), 5436–5445.

42 Y. Zhu, J. Shen, K. Zhou, C. Chen, X. Yang and C. Li, Multifunctional magnetic composite microspheres with *in situ* growth Au nanoparticles: a highly efficient catalyst system, *J. Phys. Chem. C*, 2011, **115**(5), 1614–1619.

43 A. M. El-Toni, S. Yin, T. Sato, T. Ghannam, M. Al-Hoshan and M. Al-Salhi, Erratum: investigation of photocatalytic activity and UV-shielding properties for silica coated titania nanoparticles by solvothermal coating, *J. Alloys Compd.*, 2010, **508**(1), L1–L4.

44 J. Guo, H. Van Bui, D. Valdesueiro, S. Yuan, B. Liang and J. R. Van Ommen, Suppressing the photocatalytic activity of TiO_2 nanoparticles by extremely thin Al_2O_3 films grown

by gas-phase deposition at ambient conditions, *Nanomaterials*, 2018, **8**(2), 61.

45 C. Peng, X. Yang, Y. Li, H. Yu, H. Wang and F. Peng, Hybrids of two-dimensional Ti_3C_2 and TiO_2 exposing {001} facets toward enhanced photocatalytic activity, *ACS Appl. Mater. Interfaces*, 2016, **8**(9), 6051–6060.

46 I. Rabani, R. Zafar, K. Subalakshmi, H.-S. Kim, C. Bathula and Y.-S. Seo, A facile mechanochemical preparation of Co_3O_4@g-C_3N_4 for application in supercapacitors and degradation of pollutants in water, *J. Hazard. Mater.*, 2021, **407**, 124360.

47 R. M. Mohamed, M. A. Al-Rayyani, E. S. Baeissa and I. A. Mkhalid, Nano-sized Fe-metal catalyst on ZnO–SiO_2: (photo-assisted deposition and impregnation) Synthesis routes and nanostructure characterization, *J. Alloys Compd.*, 2011, **509**(24), 6824–6828.

48 M. Sudha and M. Rajarajan, Deactivation of photocatalytically active ZnO nanoparticle by surface capping with poly vinyl pyrrolidone, *J. Appl. Chem.*, 2013, **3**, 45–53.

49 J. Wang, T. Tsuzuki, L. Sun and X. Wang, Reducing the photocatalytic activity of zinc oxide quantum dots by surface modification, *J. Am. Ceram. Soc.*, 2009, **92**(9), 2083–2088.

50 J. Wang, T. Tsuzuki, B. Tang, P. Cizek, L. Sun and X. Wang, Synthesis of silica-coated ZnO nanocomposite: the resonance structure of polyvinyl pyrrolidone (PVP) as a coupling agent, *Colloid Polym. Sci.*, 2010, **288**(18), 1705–1711.

51 J. Zhai, X. Tao, Y. Pu, X.-F. Zeng and J.-F. Chen, Core/shell structured ZnO/SiO_2 nanoparticles: preparation, characterization and photocatalytic property, *Appl. Surf. Sci.*, 2010, **257**(2), 393–397.

52 A. Morlando, V. Sencadas, D. Cardillo and K. Konstantinov, Suppression of the photocatalytic activity of TiO_2 nanoparticles encapsulated by chitosan through a spray-drying method with potential for use in sunblocking applications, *Powder Technol.*, 2018, **329**, 252–259.

53 M. C. Borrás, R. Sluyter, P. J. Barker, K. Konstantinov and S. Bakand, Y2O3 decorated TiO_2 nanoparticles: Enhanced UV attenuation and suppressed photocatalytic activity with promise for cosmetic and sunscreen applications, *J. Photochem. Photobiol., B*, 2020, 111883.

54 R. Mueen, M. Lerch, Z. Cheng and K. Konstantinov, Na-doped ZnO UV filters with reduced photocatalytic activity for sunscreen applications, *J. Mater. Sci.*, 2020, **55**(7), 2772–2786.

55 K. Lefatshe, G. T. Mola and C. M. Muiva, Reduction of hazardous reactive oxygen species (ROS) production of ZnO through Mn inclusion for possible UV-radiation shielding application, *Heliyon*, 2020, **6**(6), e04186.